Optimizing Bioengineered Vascular Systems: A Genetic Algorithm Approach

Sima Mehri, Curtis Larsen, Gregory J. Podgorski, and Nicholas S. Flann

***Abstract*—Efficient metabolism in bioengineered tissues requires a robust vascular system to provide healthy microenvironments to the cells and stroma. Such networks form spontaneously during embryogenesis from randomly distributed endothelial cells. There is a need to bioengineer endothelial cells so that network formation and operation is optimal for synthetic tissues. This work introduces a computational model that simulates *de novo* vascular development and assesses the effectiveness of the network in delivering nutrients and extracting waste from tissue. A genetic algorithm was employed to identify parameter values of the vaculogenesis model that lead to the most efficient and robust vascular structures. These parameter values control the behavior of cell-level mechanisms such as chemotaxis and adhesion. These studies demonstrate that genetic algorithms are effective at identifying model parameters that lead to near-optimal networks. This work suggests that computational modeling and optimization approaches may improve the effectiveness of engineered tissues by suggesting target cellular mechanisms for modification.**

***Key Words*—Synthetic biology, self organization, vascular development, tissue engineering, genetic algorithms, optimization, bioengineering.**

I. Introduction

Multicellular organisms depend on vascular systems for nutrient delivery and waste removal [20]. These vascular networks are formed either through vasculogenesis, a biological process in which scattered vessel precursor cells self-organize to create new networks or through angiogenesis, in which new vessels sprout from the existing vessels.

Both vasculogenesis and angiogenesis are driven primarily by chemotaxis, a mechanism in which cells move in response to a chemical gradient, along with cell-cell adhesion [19]. While many questions remain, progress in understanding and exploiting both vasculogenesis and angiogenesis is being made from a bioengineering perspective [11] [14]. Dahl et al. [23] successfully implanted tissue-engineered vascular grafts in baboons and dogs. Melero-Martin et al. [18] showed that robust development of functional vascular networks is possible *in vivo*.

With additional research in this area, bioengineered cells could be used to form functional vascular networks to create a useful delivery mechanism in synthetic tissues. However, to apply bioengineering approaches to vascular cells, genetic targets need to be identified that when modified, improve the effectiveness of the vascular systems that emerge. Given the vast number of possible targets, a method is required that could assist engineers in identifying those genetic targets.

This paper presents a proof-of-concept genetic algorithm approach to solving this problem. The genetic algorithm acts to modify a computational model of vascular network development embedded within a cell cultivation environment. The search space of the optimization are the values of model parameters which control the mechanisms of the vascular cells such as chemotaxis. Changing these parameters modifies the behavior of individual cells which ultimately influence the spatial organization of the emergent vascular network. To evaluate the quality of this network, the model simulates its operation by determining fluid flow through each vessel, and subsequent nutrient delivery to the cultured cells. The returned fitness value quantifies the total metabolic activity of culture by using bioengineered microbial cells and measuring the total product produced.

The paper is organized as follows. First, the computational model of de novo vascularization is described followed by a description of the genetic algorithm. Next, we present the results which show that genetic algorithms can identify parameter values that improve network quality. There follow details of how the network operation is simulated and the fitness function values calculated. The paper concludes with a discussion of the potential impact of this work and the remaining challenges which need to be solved to operationalize the technique.

II. Self Organizing Vascularization Model

At this proof-of-concept stage, a two-dimensional model was constructed and evaluated. Figure 1(a) illustrates the initial state of the simulated cell culture. Vessel cells (blue) that simulate the external circulatory system are arranged in two columns on both sides of the cell culture area. The left column represents the source, and the right column represents the sink, in parallel to the arterial-venous network architecture in vertebrates [21].

The tissue to be supported by the vascular network is simplified to be a field of identical cells, referred to as supported cells (yellow), randomly distributed across the area in between the two circulatory cell columns. Mixed within this field of supported cells are vascular cells (red), similar to the endothelial cells in vertebrates [19]. It is the mechanisms of the vascular cells that are to be optimized by the genetic algorithm.

During simulation, the randomly distributed vascular cells self-organize and can form a vascular network connected to both columns of circulatory cells. If this process succeeds, the supported cells will form clusters contained within each network lacuna. An example of a self-organized network is illustrated in Figure 1(b). This developmental process is described in more detail in Section II-A.

978-1-4673-8988-4/17/$31.00

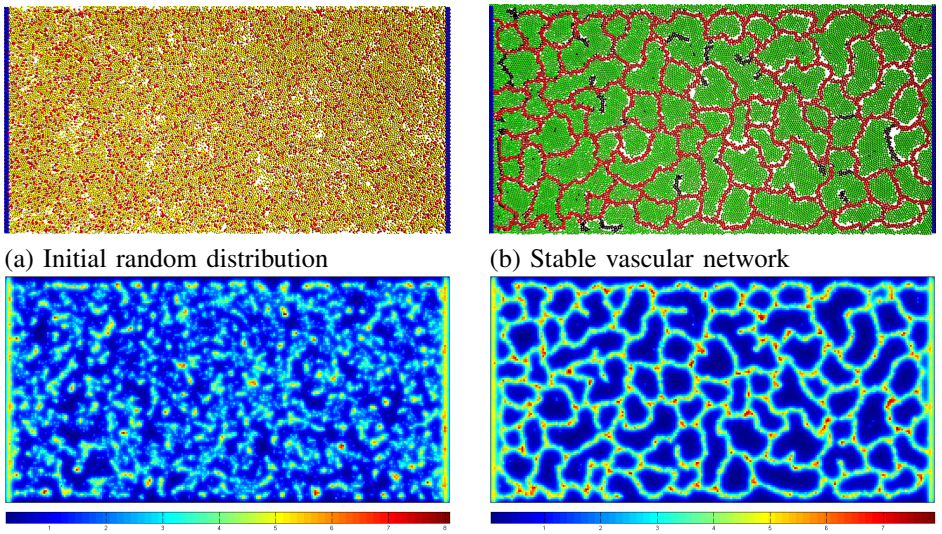

(a) Initial random distribution (b) Stable vascular network

(c) Chemoattractant during formation (d) Chemoattractant state distribution

Fig. 1: **Self-organizing Network**: (a) is the initial conditions with fixed circulatory cells (blue) on each side and vascular (red) and supported cells (yellow) randomly mixed; (b) is the steady state network following self organization; (c) is the distribution of chemoattractant during vessel formation and (d) is at a steady state. In all images of biochemical distribution, blue signifies a low concentration, while red signifies a high concentration.

To evaluate the performance of the network, first an estimate of the flow through the vascular system is calculated and then the vascular network operation is simulated. As the network provides nutrients, the supported cells become active (turn green in the figures) and consume nutrients and secrete wastes. Note that in this case the network fitness would be high because almost all of the supported cells are active and close to a vessel. This network operational process is described in more detail in Section V.

A. De Novo Vascularization Model

The two key cellular mechanisms in vascularization are chemotaxis, where cells move in respond to chemical gradients, and tight junctions, where adjacent cells form strong bonds. Cells are modeled as particles that can secrete and respond to chemicals and move in response to forces. The modeling framework is based on iDynamics [12] originally created for biofilm models.

Initially, the particles representing epithelial cells are placed randomly in the simulation domain mixed with the support cells. A chemotactic nutrient is initially supplied at concentration N_c, set at $8.9 \times 10^{-8} m^{-2}$. The fixed cells on the sides of the cell culture secrete C_{long}, a chemoattractant with small decay rate, and C_{short}, a chemoattractant with a large decay rate. The moving cells within the culture only secrete C_{short}. The decay rates affect the shape of the chemoattractant gradient. C_{short} is a localized concentration with a sharp gradient, and C_{long} has a long-distance shallow gradient. The concentrations of each are described by the Monod-kinetic reaction in Equation 1. D_c of both chemoattractants are set to $1 \times 10^{-13} m^2 s^{-1}$ as given in the in-vitro angiogenesis study of Merks et al [19]; β is the decay rate; M is the mass of the secreting cell; k is the Monod-kinetic coefficient; μ is the maximum secretion rate.

$$\frac{\partial C}{\partial t} = D_c \bigtriangledown^2 C + \mu \frac{N_c}{(N_c + k)} M - \beta C \tag{1}$$

The moving cells respond to the gradient of the chemoattractants by tending to towards higher concentrations in a process described in Equation 2 and by Adler [1]. Let p be a particle that responds to chemoattractant C. A random unit vector $\vec{c}$ is generated and considered as a potential chemotactic force on p. The local gradient of chemoattractant across p in direction $\vec{c}$ is determined by sampling C ahead of p, referred to as C^+, and behind p, referred to as C^-. The magnitude of force F in direction $\vec{c}$ is given by the equation 2 [19], where λ is the parameter that controls the magnitude of the response to the gradient and α controls saturation of the chemotactic force. The force F is only applied to the particle if greater than zero.

$$F = \lambda \Big(\frac{C^+}{1 + \alpha C^+} - \frac{C^-}{1 + \alpha C^-} \Big) \tag{2}$$

Adhesive forces act among the particles and are attractive at close distances and neutral otherwise. In this work, endothelial cell-cell adhesion is strong and endothelial-supported cell is weak. When endothelial cells become close, tight junctions begin to form, binding the cells together as a precursor to vessel construction. In the model, if two adjacent cells form a tight junction, then a stiff spring connects the corresponding particles.

In addition to chemotactic force $F \cdot \vec{c}$, each particle experiences forces due to non-overlapping constraints caused by competition for space. Once the net forces have been assigned to each particle, the system is relaxed by a shoving algorithm which moves the particles along their force vectors to minimize stress. In this way, the vessel particles push through the supported particles, form clumps due to attractive chemotactic forces, and then buckle and extend immature vessels. The system can eventually reach the morphology illustrated in Figure 1(b), in which all biomechanical forces are relaxed, and concentrations of molecules are stable, see Figure 1(d).

TABLE I: Known parameter descriptions

Parameter	Value	Description
D_c	$1 \times 10^{-13} m^2 s^{-1}$	Chemoattractant Diffusion coefficient
N_c	$3 \times 10 g L^{-1}$	Chemoattractant nutrient concentration
M_{fixed}	$1 \times 10^{-11} g$	Mass of fixed epithelial cells
M_{moving}	$1 \times 10^{-11} g$	Mass of moving epithelial cells
α	0.1	Saturation of chemotactic force

III. The Genetic Algorithm

The self organizing vascular model has seven parameters with unknown values (Table II). The best fit for these parameters was found using a genetic algorithm from the Java Genetic Algorithms Package [17]. The seven parameters are used as genes in individual chromosomes. The initial population had a size of three and was constructed by random selection of parameter values from the ranges shown in Table II. As the population evolves during runs of the genetic algorithm, each individual is evaluated using the parameter values encoded in the genes used to run the vascular model (see Section II for more details). The resulting vascular network is then evaluated as described in Section V, and the fitness is assigned based on the metabolic production. Next, genetic operators were run on the population followed by a re-evaluation of the population that now contained new individuals. Finally, selection was applied to obtain the new population for the next round of evolution. Crossover and mutation operators were included in the genetic algorithm, with the crossover operator applied to 35% of the population per generation and the mutation operator was applied to each gene with a probability of 1/12. An elitist ranking selector cloned the top %90 of the population, with the remaining 10% of the population filled with the same individuals in the order of fitness. The results presented in this paper were obtained using 1000 steps of evolution.

IV. Results

Initial runs of the algorithm were performed on a two dimensional cellular culture. Its height was set to 0.768 mm while the width was fixed at 1.536 mm. The total number of supported and vascular cells were 4200 and 1800, respectively where vascular cells contributed to 30 per cent of total number of cells. A total of 384 circulatory cells simulating the external delivery and metabolic product extraction system

TABLE II: Parameters searched by the GA

Parameter	Low	High	Description
k	10^{-10}	10^{-2}	Monod-kinetic coefficient
μ_{short}	1	7	Secretion rate of C_{short}
μ_{long}	1	7	Secretion rate of C_{long}
β_{short}	10^{-5}	10^{-1}	Decay rate of C_{short}
β_{long}	10^{-10}	10^{-3}	Decay rate of C_{long}
λ_{short}	1	6	Chemoattractant response to C_{short}
λ_{long}	1	6	Chemoattractant response to C_{long}

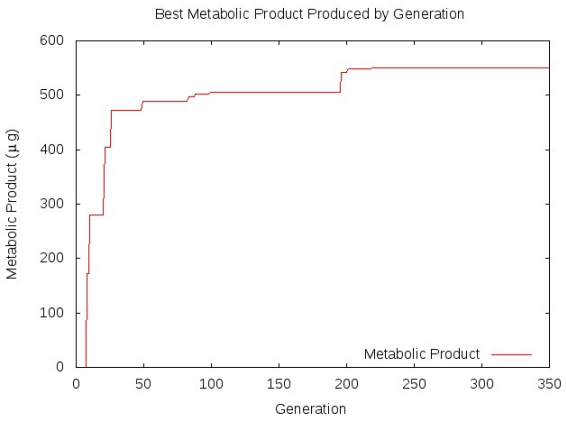

Fig. 2: The metabolic production of the best-so-far individual identified as a function of generation. Only a single run is provided due to the four hours needed for each fitness evaluation.

is implemented as two identical columns on two sides of the cellular culture. The number of all mentioned cells were kept constant through the experiment. The simulations started with a random distribution of supported and vascular cells inside the culture. Sixteen simulated hours are allocated for network development, after which the network's quality is evaluated. If no path of vessels is found that connects the source to the sink, then the fitness score is set at zero. Otherwise, the fitness score of the network is estimated by measuring the metabolic productivity of the supported cells while simulating the operation of the vascular network for two simulated hours. This process is described in detail in Section V.

Figure 2 shows the best case fitness of the networks produced during the running of the genetic algorithm. The algorithm starts with random values for the chosen parameter within the given ranges. As shown in the graph, the GA is unsuccessful in creating a productive cell culture for the first several evolutions. However, once it finds a parameter set leading to a functioning network, it continually improves the quality of solutions. After 1,000 iterations, the highest fitness level was 537.66 μg of product production. The parameter values contributing to the best case are shown in Table III.

Figure 3 shows some sample cell cultures produced by the genetic algorithm during its evolution. As it is seen in the figure, some arrangements of the vascular cells do not form a network for the flow of material and thus no production is obtained in the system. Figure 3 (a) depicts a cell culture with

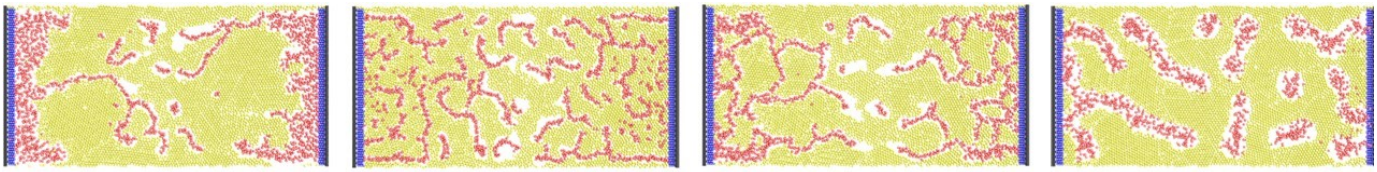

(a) (b) (c) (d)

Fig. 3: Sample results of the GA during its evolution. These results show unsuccessful attempts of the GA at creating a consistent vascular network for the flow of nutrients and products

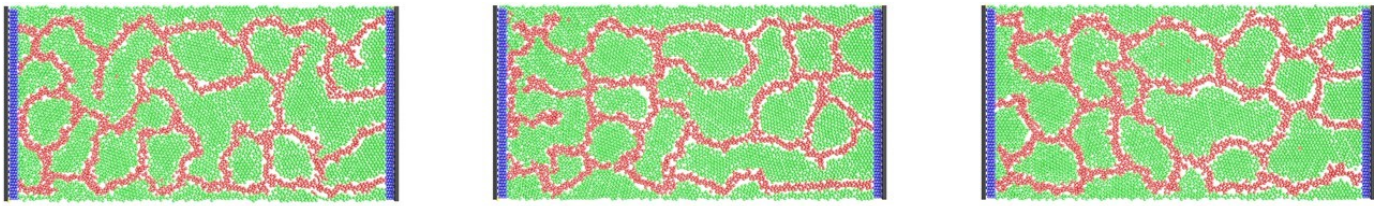

(a) (b) (c)

Fig. 4: A sample of best solutions identified by the genetic algorithm during evolution. These results depict vascular networks that have successfully nourished the supported cells along with removing their products and waste

TABLE III: The best parameter values found by the GA

k	6.78×10^{-3}	Monod-kinetic coefficient
μ_{short}	5.12	Secretion rate of C_{short}
μ_{long}	6.10	Secretion rate of C_{long}
β_{short}	67.3×10^{-3}	Decay rate of C_{short}
β_{long}	7.41×10^{-6}	Decay rate of C_{short}
λ_{short}	2.69	Chemoattractant response to C_{short}
λ_{long}	1.99	Chemoattractant response to C_{long}

most of the vascular cells accumulated beside the circulatory cells on the sides and occasional formations in the middle. This can be a result of high chemotactic response to C_{long} and α.

Figures 3 (b) and (d) both demonstrate scattered and disconnected lines of vascular cells floating among supported cells. Such arrangements result from a low amount of C_{long} but a high amount of β_{short}. It should be mentioned that the cell culture in Figure 3 (d) has a higher β_{short} than the one in 3 (b) which accounts for the thicker lines of vascular cells. On the other hand, Figure 3 (c) shows another unsupported cell culture with several cycles of vascular cells but no path connecting the source to the sink. This result follows from low λ_{short} and high λ_{long} and μ_{long}.

Figure 4 depicts cellular cultures found by the GA that have successfully formed networks of vascular cells and reached the highest amount of production. No patches of yellow non-producing cells are present in these cell cultures. As depicted, vascular cells have successfully formed a number of lacunae that feed all supported cells available in the culture and move waste and products away. More lacunae of vascular cells means availability of nutrients to more supported cells and therefore, higher production. Investigating the parameters leading to these solutions reveal an average amount of λ_{short} and λ_{long} and low amounts of μ_{short}, μ_{long}, β_{short}, β_{long} and k. There are few unconnected branches stretching from a few points which given a larger time frame could lead to more lacunae and even a higher production. The exact amount of each parameter for cultures depicted in Figures 3 is given in Table IV. For comparison purposes, the parameter values for Figure 4(a) is also given in the same table.

V. Fitness of a Vascular System

The quality of the network is evaluated by determining the flow through each branch and modeling the release of nutrients and the capture of secretions from the supported cells. A full description of the functioning vascular model and its derivation is given in [4]. To assess the health of the supported cells given a running vascular network, the rate of metabolism of each supported cell is estimated by measuring how efficiently the cells produce some arbitrary product, X, described by Equation 3.

$$\frac{\partial X}{\partial t} = +\mu_p \frac{N}{(N+k_p)} \frac{k_i}{(X+k_i)} M_p + D_p \bigtriangledown^2 X \qquad (3)$$

Where M_p is supported cell biomass. To produce a realistic model of cellular metabolism, the parameter values of the supported cells is replicated from [3] and is based on vanillin production of Pycnoporus cinnabarinus. The product X is secreted by the supported cells consuming nutrient N following Michaelis-Menten kinetics with a reaction rate of μ_p, where the saturation of enzymes involved in the X production is considered k_p. The negative feedback due to product inhibition is also taken into account, with a correspondent inhibitor constant k_i [6], [13] and [2].

TABLE IV: Parameter Table Corresponding to cellular cultures depicted in Figures 3 and 4

Culture	λ_{short}	λ_{long}	μ_{short}	μ_{long}	β_{short}	β_{long}	k
Figure 3-(a)	1.28	4.09	5.90	6.58	6.79×10^{-2}	5.96×10^{-4}	2.64×10^{-3}
Figure 3-(b)	1.28	5.92	5.90	5.21	6.79×10^{-2}	8.54×10^{-4}	8.96×10^{-3}
Figure 3-(c)	1.11	1.22	6.69	4.50	9.90×10^{-2}	2.06×10^{-4}	1.49×10^{-3}
Figure 3-(d)	5.73	1.22	6.69	4.50	8.14×10^{-2}	5.70×10^{-4}	2.17×10^{-3}
Figure 4	2.69	1.34	3.85	6.10	3.23×10^{-2}	7.68×10^{-5}	2.64×10^{-4}

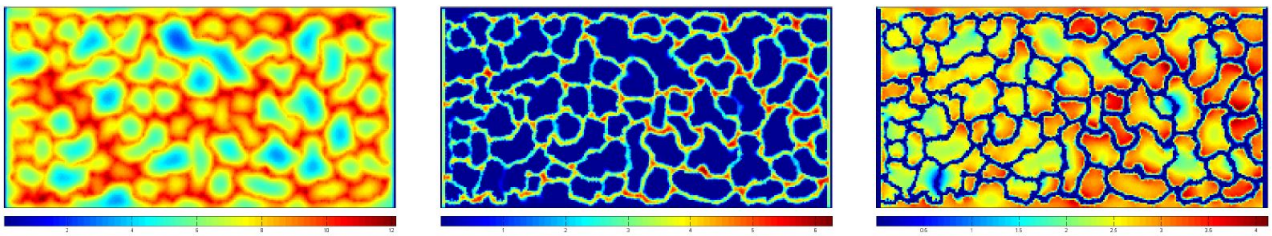

(a) Early N distribution (b) Stable state N distribution (c) Stable state X distrubution

Fig. 5: **Cell culture activation**: The distribution of nutrient (a) when the vessel flow begins, but the supported cells are not yet active, (b) at steady state nutrient distribution when the supported cells are active; note that all extra-vessel nutrient is consumed, (c) the product distribution when the supported cells are active.

Nutrient will be consumed by the supported cells in direct correspondence to the production of X, but at a different reaction rate μ_n:

$$\frac{\partial N}{\partial t} = -\mu_n \frac{N}{(N + k_p)} \frac{k_i}{(k_i + X)} M_p + D_p \bigtriangledown^2 N \qquad (4)$$

Figure 5 illustrates the distribution of nutrient and product during simulated network operation for the network illustrated in Figure 1(c). Figure 5(a) illustrates the nutrient distribution before the supported cells have become active. In Figure 5(b) gives the nutrient distribution following supported cell activation. In Figure 5(c) the distribution of the product is illustrated. Note the regions of low product (the blue areas) where the vascular flow is limited.

The final step is to integrate the amount of X extracted from the cellular culture by the vascular network over a fixed period, in this case two hours. This accumulation of product will be a function of the aggregate metabolic rate of the supported cells. It is this value the simulator returns as the fitness score of the vascular network architecture.

VI. Discussion

This work explored a solution to the problem faced by bioengineers to determine those cellular mechanisms to target for modification when improving vascularization for synthetic tissue engineering. The method integrated a hybrid particle-based model of vascularization as a fitness function with a genetic algorithm applied to optimize the search space of model parameter values. The method is generic in that models of different biological systems could be substituted for vascularization and the fitness function likewise changed to reflect alternative objectives, such as minimizing vascular function to combat tumor growth in cancer [15].

In this initial study, the search space was reduced to only consider parameters that influence the chemotactic mechanism of the vascular cells. Previous work with the model identified the importance of adhesion and tight junction formation in robust network formation. However, increasing the number of parameters to include these cellular mechanisms would significantly increase the search space, resulting in many more fitness function calls. Given the modeling framework employed here [12], this is currently impractical because each fitness evaluation takes at least four hours of CPU time running on a 3.6 GHz machine. Recently two fast large-scale simulation systems have been developed by Ghaffarizadeh et al. [5] and *Biocellion* [9]. Both these systems implement an individual-based approach similar to *cDynoMiCs* employed here. *Biocellion* is implemented as a distributed architecture executable on the Cloud [7] and is capable of simulating complex 3D models of billions of cells in a matter of a few hours. *Biocellion* has the potential to simulate vascularization quickly enabling the optimization of more complex bioengineered multicellular systems.

The principle challenge in bringing this work to practicality is to operationalize the link between model parameters and actual genetic sequences. If this can be achieved, then the output of the optimization process could be directly mapped to engineering targets in the genome. In traditional bioengineering where products are produced in biofactories [22], [24], targets are identified through analysis of detailed metabolic models of microbial cells, such as [10]. The functioning of

mammalian cells is less understood, particularly mechanisms such as chemotaxis that are unrelated to metabolic processes, which can be modeled using flux balance analysis.

The key to operationalizing bioengineering of multicellular systems is to utilize multiscale models of the biological system under study. Multiscale models link the mechanisms acting at different spatial and temporal scales together into an integrated system where changes in expression and regulation of genes are manifested in large-scale multicellular outcomes [16], [8] [26]. If such detailed models were employed, the high-level abstract parameters of this work would be replaced by specific genetic mechanisms resulting in solutions being mapped directly to genetic targets.

VII. Conclusions

This work has shown that genetic algorithms are sufficiently powerful to optimize complex biological systems, even when there is a non-linear relationship between the parameters and the fitness function. This method can be applied to models of different biological systems that consider alternative objectives.

Many challenges exist before this optimization approach can be applied to actual bioengineered tissues. Two principle challenges are that (a) the speed of the simulations needs to be increased to allow expansion of the parameter space and to increase the fidelity of the model, and (b) methods to engineer the molecules that influence vascular tissue organization to meet the predicted optimal parameter values must be expanded and improved. However, although not all the molecules considered in this work can yet be easily tuned to meet optimal parameter values, existing real-world approaches are available for at least some of them. For example, the secretion rate of the chemoattractants can potentially be altered by changing the intracellular stability of genetically engineered chemoattractants guided by the N-end rule [25]. Similarly, there is the possibility of increasing the decay rate of both the short-range and long-range chemoattractants by adding selective targets of specific proteases that could be introduced into the culture system. Exploring these modifications may move this in silico system to an in vitro system with practical applications.

Acknowledgment

This work was supported by the Luxembourg Centre for Systems Biomedicine, the University of Luxembourg and the Institute for Systems Biology, Seattle, USA. Research reported in this publication was partially supported by the National Institute Of General Medical Sciences of the National Institutes of Health under Award Number P50GM076547. The content is solely the responsibility of the authors and does not necessarily represent the official views of the National Institutes of Health.

References

[1] Julius Adler. Chemotaxis in Escherichia coli. *Cold Spring Harbor Symposia on Quantitative Biology*, 30:289–292, January 1965.

[2] S. Aiba, M. Shoda, and M. Nagatani. Kinetics of product inhibition in alcohol fermentation. *Biotechnol. Bioeng.*, 10(6):845–864, November 1968.

[3] Olivier Bernard, Georges Bastin, Christelle Stentelaire, Laurence Lesage-Meessen, and Marcel Asther. Mass balance modeling of vanillin production from vanillic acid by cultures of the fungus Pycnoporus cinnabarinus in bioreactors. *Biotechnol. Bioeng.*, 65(5):558–571, December 1999.

[4] Delin Davis, Anna Doloman, Gregory J. Podgorski, Elizabeth Vargis, and Nicholas S. Flann. Exploiting Self-organization in Bioengineered Systems: A Computational Approach. *Frontiers in Bioengineering and Biotechnology*, 5, April 2017.

[5] Ahmadreza Ghaffarizadeh, Samuel H. Friedman, and Paul Macklin. Agent-based simulation of large tumors in 3-D microenvironments. *bioRxiv*, page 035733, 2015.

[6] Keehyun Han and Octave Levenspiel. Extended monod kinetics for substrate, product, and cell inhibition. *Biotechnol. Bioeng.*, 32(4):430–447, August 1988.

[7] Ibrahim A. Hashem, Ibrar Yaqoob, Nor B. Anuar, Salimah Mokhtar, Abdullah Gani, and Samee Ullah Khan. The rise of big data on cloud computing: Review and open research issues. *Information Systems*, 47:98–115, January 2015.

[8] Jason A. Joseph Walpole. Multiscale Computational Models of Complex Biological Systems — Annual Review of Biomedical Engineering. *Annual Review of Biomedical Engineering*, q5:137–154, 2013.

[9] Seunghwa Kang, Simon Kahan, Jason McDermott, Nicholas Flann, and Ilya Shmulevich. Biocellion: accelerating computer simulation of multicellular biological system models. *Bioinformatics (Oxford, England)*, 30(21):3101–3108, November 2014.

[10] Peter D. Karp, Mario Latendresse, Suzanne M. Paley, Markus Krummenacker Quang Ong, Richard Billington, Anamika Kothari, Daniel Weaver, Tom Lee, Pallavi Subhraveti, Aaron Spaulding, Carol Fulcher, Ingrid M. Keseler, and Ron Caspi. Pathway Tools version 19.0: Integrated Software for Pathway/Genome Informatics and Systems Biology, October 2015.

[11] Tamar Kaully, Keren Kaufman-Francis, Ayelet Lesman, and Shulamit Levenberg. VascularizationThe Conduit to Viable Engineered Tissues. *Tissue Engineering Part B: Reviews*, 15(2):159–169, March 2009.

[12] Laurent A. Lardon, Brian V. Merkey, Sónia Martins, Andreas Dötsch, Cristian Picioreanu, Jan-Ulrich Kreft, and Barth F. Smets. iDynoMiCS: next-generation individual-based modelling of biofilms. *Environmental Microbiology*, 13(9):2416–2434, September 2011.

[13] Octave Levenspiel. The monod equation: A revisit and a generalization to product inhibition situations. *Biotechnol. Bioeng.*, 22(8):1671–1687, August 1980.

[14] Michael Lovett, Kyongbum Lee, Aurelie Edwards, and David L. Kaplan. Vascularization Strategies for Tissue Engineering. *Tissue Engineering Part B: Reviews*, 15(3):353–370, June 2009.

[15] Arthur W. Mahoney, Gregory J. Podgorski, and Nicholas S. Flann. A Multi-Objective Optimization Based-Approach for Discovering Novel Cancer Therapies. *IEEE/ACM Transactions on Computational Biology and Bioinformatics*, Preprint, April 2010.

[16] M. L. Martins, S. C. Ferreira, and M. J. Vilela. Multiscale models for biological systems. *Current Opinion in Colloid & Interface Science*, 15(1-2):18–23, April 2010.

[17] Klaus Meffert. Java genetic algorithms package, 2011.

[18] Juan M. Melero-Martin, Maria E. De Obaldia, Soo-Young Kang, Zia A. Khan, Lei Yuan, Peter Oettgen, and Joyce Bischoff. Engineering Robust and Functional Vascular Networks In Vivo With Human Adult and Cord BloodDerived Progenitor Cells. *Circulation Research*, 103(2):194–202, July 2008.

[19] Roeland M. H. Merks, Erica D. Perryn, Abbas Shirinifard, and James A. Glazier. Contact-Inhibited Chemotaxis in De Novo and Sprouting Blood-Vessel Growth. *PLoS Comput Biol*, 4(9):e1000163+, September 2008.

[20] R. Monahan-Earley, A. M. Dvorak, and W. C. Aird. Evolutionary origins of the blood vascular system and endothelium. *Journal of thrombosis and haemostasis : JTH*, 11 Suppl 1:46–66, June 2013.

[21] Carl L. Reiber and Iain J. McGaw. A Review of the Open and Closed Circulatory Systems: New Terminology for Complex Invertebrate Circulatory Systems in Light of Current Findings. *International Journal of Zoology*, 2009:1–8, 2009.

[22] R. Sharma, Y. Chisti, and U. C. Banerjee. Production, purification, characterization, and applications of lipases. *Biotechnology advances*, 19(8):627–662, December 2001.

[23] Takanori Takebe, Naoto Koike, Keisuke Sekine, Ryoji Fujiwara, Takeru Amiya, Yun-Wen W. Zheng, and Hideki Taniguchi. Engineering of human hepatic tissue with functional vascular networks. *Organogenesis*, 10(2):260–267, 2014.

[24] Jan Maarten M. van Dijl and Michael Hecker. Bacillus subtilis: from soil bacterium to super-secreting cell factory. *Microbial cell factories*, 12, 2013.

[25] Alexander Varshavsky. The N-end rule pathway and regulation by proteolysis. *Protein science : a publication of the Protein Society*, 20(8):1298–1345, August 2011.

[26] Jessica S. Yu and Neda Bagheri. Multi-class and multi-scale models of complex biological phenomena. *Current Opinion in Biotechnology*, 39:167–173, June 2016.